Available online at www.sciencedirect.com

Pediatric Dental Journal

journal homepage: www.elsevier.com/locate/pdj

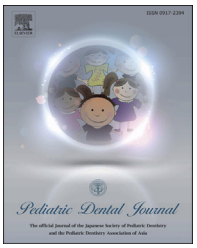

Research Paper

Progress of LPS-induced apical lesion in rat immature mandibular molars

Chikako Nakajima [a,1], *Maiko Fujita-Otani* [a,1], *Yuko Mikuni-Takagaki* [b,*], *Kuniomi Nakamura* [a], *Kouki Hidaka* [c], *Akira Kawata* [d], *Ryota Kawamata* [e], *Shigenari Kimoto* [a]

[a] *Department of Pediatric Dentistry, Kanagawa Dental University, Yokosuka, Japan*
[b] *Kanagawa Dental University, Yokosuka, Japan*
[c] *Department of Restrative Dentistry, Kanagawa Dental University, Yokosuka, Japan*
[d] *Department of Pathology and Histomorphology, Kanagawa Dental University, Yokosuka, Japan*
[e] *Division of International Dentistry, Department of Comprehensive Dentistry, Kanagawa Dental University, Yokosuka, Japan*

ARTICLE INFO

Article history:
Received 7 November 2022
Received in revised form
14 December 2022
Accepted 22 December 2022
Available online xxx

Keywords:
Immature Teeth
Root closure
M2 macrophage
Lipopolysaccharide
Periapical periodontitis

ABSTRACT

Introduction: The objective was to assess the process of apical periodontitis induced by injecting *Porphyromonas gingivalis* lipopolysaccharide (Pg LPS) that is followed by regeneration of roots in premature permanent tooth. A novel operation table was introduced to facilitate endodontic treatment of mandibular molars.

Materials and Methods: Pulp of mandibular first molars of 6-week Wistar rats were exposed by drilling, inoculated with 0.6 μg Pg LPS and sealed with glass ionomer cement. After 1 and 2 weeks rats were sacrificed and the molar roots compared with those of vehicle controls by protein array analysis and (histo) morphology/chemistry. Micro-CT imaging visualized the lesion, and non-decalcified frozen serial sections were HE stained and subjected to TRACP-5b/ALP activity staining and immunohistochemical staining.

Results: Quantitative induction of inflammation enabled us to examine the effects of LPS-injection: micro-CT images exhibited much larger radiolucent apical lesions than did controls; CD68 (M1+ M2±) cell surface marker was more intense in Pg-1w and then subsided while CD163 (M1- M2+) was more intense in Pg-2w. Staining of IL-4, which induces M2 polarization, and angiogenic markers, VEGF/CD34 was intense in Pg-1w than in controls.

Conclusion: The introduced apparatus facilitated accurate mandible operation with ease. Thus, stages of pulpal infection were reproduced quantitatively with a small amount of Pg LPS. Proteins expressed in the root apex where inflammation occurred and the lesion in the surrounding alveolar bone revealed the inflammation time course in the immature permanent teeth. This mandibular model turned out quite useful for clinical and pharmaceutical developments in the future.

* *Corresponding author.*
E-mail address: takagaki@kdu.ac.jp (Y. Mikuni-Takagaki).
[1] These two authors contributed equally.

https://doi.org/10.1016/j.pdj.2022.12.001
0917-2394/

Please cite this article as: Nakajima C et al., Progress of LPS-induced apical lesion in rat immature mandibular molars, Pediatric Dental Journal, https://doi.org/10.1016/j.pdj.2022.12.001

1. Introduction

In daily practice, dentists are often required to perform endodontic treatment in immature permanent teeth such as those with a fractured central tubercle. The roots of immature permanent teeth are usually incomplete with a funnel-shaped apex making treatment difficult. A central tubercle is an abnormal form of crown that appears mainly on the central portion of the occlusal surface of premolars, more commonly in mongoloids. It has been reported to form in about 1% of Japanese [1] and to be found mostly in mandibular second premolars [1–4]. Fractures generally occur during the process of tooth eruption necessitating attention to prevent dental pulp infection through fracture cracks [5]. Currently, there is no agreed standard treatment to aid root development to complete the process. This is an urgent task to establish a reliable protocol leading to normal permanent teeth with mature roots. The goal of endodontic treatment of such immature teeth is to preserve their function as much as possible.

Animal models have been used in evaluating certain pathogenesis, identifying the actions of novel drugs, and determining the results of interventions prior to clinical trials. To date, dental experiments have often used rat maxillary molars [6–8] rather than mandibles because of anatomical constraints with cheek, tongue, and pericranial tissues associated with rat mandible. While few studies used mandibular teeth, certain clinical conditions such as central tubercle fracture necessitate use of mandibular teeth models.

Infection of periapical tissues may occur by pathogenic invasion of microorganisms into the dental pulp during dental caries, trauma or other ailments. Inflammatory reaction in periapical tissues is induced by microbial infection in the root canal system [9]. Resulting root apex periodontitis is an inflammatory disease characterized by reduced periodontal tissue and alveolar bone. Apical periodontitis models prepared by surgically exposing dental pulp have been widely used, mostly with rats whose dental pulp was left open and exposed to oral bacteria. Infected pulpal tissue was then used as a periodontitis model [10,11]. It is difficult to identify the source and extent of an infection occurred at the root apex in such a model. On the other hand, by injecting a pathogen directly into the dental pulp and sealing it with glass ionomer cement, one can control the source and determine the extent of induced inflammation followed by healing to obtain an apical periodontitis model. To perform such an operation on mandibular teeth of young rats, is challenging, however.

In the present study, we developed apparatus, a table, to facilitate easy operation on rat mandibular molars which may be used to develop mandibular teeth models. Using this novel operation table, we examined the effect of *Porphyromonas gingivalis* lipopolysaccharide (Pg LPS) injected into the pulp of mandibular first molar teeth. The effects were assessed at 1-week (Pg-1w) and 2-weeks (Pg-2w) post-inoculation by micro CT imaging, antibody array, activity staining for ALP and TRACP-5b and immunofluorescence staining. We obtained useful information with regard to the process of inflammation leading to healing that could contribute to the development of new treatment methods.

2. Materials and Methods

2.1. Animals

Wistar rats (n = 48 in all, 8 groups of 6 rats; 5-week-old male rats weighing about 130 g purchased from Japan SLC, Shizuoka, Japan) were operated on after 1-week habituation at constant room temperature (22 ± 3 °C), relative humidity (55 ± 5%), under a 12 h day/night cycle (lights on 7 p.m. to 7 a.m.), with food and water *ad libitum*. All animal experiments accorded with Guidelines for Animal Experiments, Kanagawa Dental University, and every effort to minimize animal suffering was made. The experimental procedures were approved by Animal Experiment Committee, Kanagawa Dental University (No. 21–014). The rats were randomly divided into experimental and control (Ctrl) groups. All were anesthetized with chloral hydrate (0.33 ml/kg) via intraperitoneal administration, prior to operation.

2.2. Operating table

A rat strapped to the operating table created to treat mandibular molars in young rats is shown in Fig. 1A. During use of the device, moisture in the oral cavity was controlled with rubber dam clamps for rats (YDM, Tokyo, Japan) and rubber dam sheets for small animals (J. Morita Corp, Osaka, Japan), and the operative field was disinfected with 0.025% benzalkonium chloride solution prior to operation.

After cleaning the pulp chamber with saline solution and then sodium hypochlorite solution.

2.3. Induction of periapical lesions and sample preparation

The pulp of the mandibular right first molar was exposed by drilling with a sterilized ELAsteel/HP/1/4 diamond bur (Emil Lange, Engelskirchen, Germany) until the bur head sank into the pulp chamber under observation with a surgical loupe (Japan Dental Supply Corp. Tokyo, Japan). After cleaning the pulp chamber with saline solution and then sodium hypochlorite solution, 0.6 μl of the prepared treatment medium comprising *Porphyromonas gingivalis* lipopolysaccharide (Pg-LPS) (InvivoGen, San Diego, USA) dissolved in sterile endotoxin-free water at 1 μg/μl concentration was directly injected towards the bottom of the pulp chamber, using a micro syringe (0–5 μl) fitted with a 1.5 cm long 33-gauge needle (ITO CORPORATION, Shizuoka, Japan). Ctrl rats were injected with 0.3 μl sterile endotoxin free water. The syringe was left in situ for 30 s after each injection. The pulp chamber was then capped with glass ionomer cement (YOSHIDA CO., LTD., Tokyo, Japan). In each animal, the opposite left-side tooth was not treated and served as an intact reference (data not shown). Six treatment rat groups (Pg-1w), another six treatment rat groups (Pg-2w) were maintained together with the Ctrl rat groups under the same conditions and then sacrificed with CO_2 gas. The mandibles containing the first molar samples were cut out and trimmed, fixed with 4% paraformaldehyde in phosphate-

Please cite this article as: Nakajima C et al., Progress of LPS-induced apical lesion in rat immature mandibular molars, Pediatric Dental Journal, https://doi.org/10.1016/j.pdj.2022.12.001

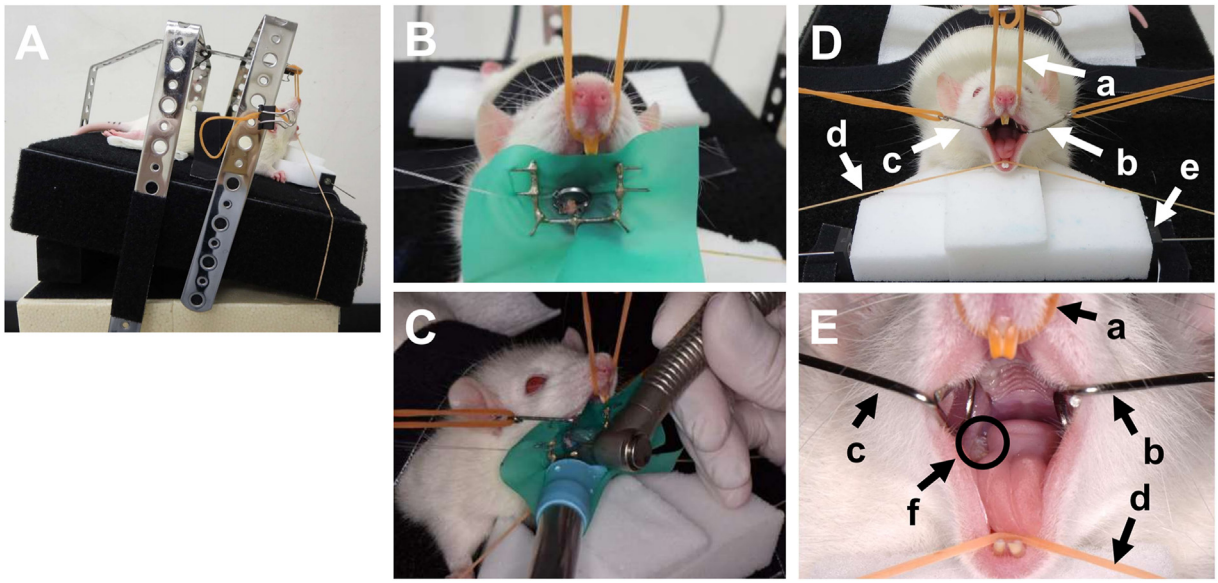

Fig. 1 – Overall view of the operating table and rubber dam isolation. The table shown in Fig. 1A comprising three metal mesh plates W20 × L20 × H5 (cm) may be adjusted in height (A). Rubber dam isolation (B) and treatment of mandibular molar teeth (C). With the rubber dam dry field technique, molars are easily accessible. Stabilized head facilitates accurate operation. There are four directions of traction (D and E). (a: maxilla incisor traction, b: left buccal mucosa traction, c: right buccal mucosa traction, d: mandible incisor traction). Mandibular fixation (e) and intraoral viewing are simple. First molars (f) can be easily accessed.

buffered saline (pH 7.4) (NACALAI TESQUE, INC., Kyoto, Japan) at 4 °C for 48 h with two changes. Samples were further transferred into 70% ethanol, and after replacing the ethanol solution twice, refrigerated until imaging and histological analyses.

2.4. *Three-dimensional measurement of root canal lesions*

The mandibular first molar roots were scanned and visualized with a micro-CT scanner (ScanXmate-L80, Comscantechno, Yokohama, Japan). The micro-CT, which visualizes the microstructure of hard tissue, is useful for evaluating root apex condition. Reconstructed 3D images of the mandible showing the microstructure of the root canal lesion provided data to quantify the volume of bone resorption in the lesion as transmission images. The image data were reconstructed using TRI/3D-BON (RATOC System Engineering, Tokyo, Japan). The volumes of periapical lesions at the mesial and distal roots were calculated by Image J (U.S. National Institutes of Health, Bethesda, Maryland, USA). The imaging conditions were 50 kV tube voltage, 60 μA tube current, and 30 μm slice width. For each imaging data, the X axis passed through the floor of the pulp bed, the Y axis passed through the centers of the proximal and distal roots, and the Z axis passed through the centers of the buccal and lingual roots. The volume of root apex transparency in each slice was defined as the area of transparency multiplied by the slice width, and the cumulative total was calculated for the root apex transparency image volume. Mesial and distal roots showed similar tendency between the results of Pg and Ctrl groups.

2.5. *Protein array*

To analyze tissue protein in the area of root apex-alveolar bone resorption, the base of the pulp under removed teeth was recovered immediately after sacrifice in the rats separately prepared for the protein array experiment after 2-week incubation. By repeated flashing using a tuberculin syringe with 180 μl lysis buffer divided in three portions (RayBiotech Life, Inc., Peachtree Corners, GA.), tissue proteins were collected into Eppendorf tubes. In between the flashing treatments, alveolar bone surfaces in the lesion were scraped with the needle's cutting edge to recover proteins. Concentrations of the recovered proteins were determined using Pierce 660 assay (Thermo-Fisher Scientific, Tokyo, Japan) with BSA as a standard, then frozen at −130 °C for further analyses.

For simultaneous detection of the relative expression of 500 rat proteins in the tissue lysates, RayBio® label-based (L-Series) rat L2 array on glass slides (Ray Biotech Life, Inc. Peachtree Corners, GA) was according to the manufacturer's instructions. Briefly, primary amine groups in the sample proteins were biotinylated, and the glass slide arrays were first treated with blocking solution similar to that used in Western blot analysis. Then a solution of biotin-labeled sample was added onto the glass slide, which was preprinted with captured antibodies. After the slide was incubated to allow binding of target proteins, streptavidin-conjugated fluorescent dye (Cy3 equivalent) was applied to the array. After washing the dye off the glass slide, dried slides were skimmed through a fluorescence scanner to visualize the signals. Depending on the intensity, the presence of each protein was semi-quantitatively estimated.

Please cite this article as: Nakajima C et al., Progress of LPS-induced apical lesion in rat immature mandibular molars, Pediatric Dental Journal, https://doi.org/10.1016/j.pdj.2022.12.001

2.6. Histology

Blocks fixed and kept in 70% ethanol were transferred into 10% sucrose, and after two changes each of 10% and 20% sucrose at 4 °C, dipped in a small volume of freezing medium (SECTION-LAB Co. Ltd., Hiroshima, Japan). The blocks were then submerged in metal containers filled with the freezing medium and were frozen according to Kawamoto's protocol slightly modified in our previous study [12]. Four-μm thick serial sections in the sagittal plane of the teeth were prepared so that apical foramen (AF), root canal (RC), periapical lesion (PL), and alveolar bone (AB) can be seen. Sections from the center portion of the pulp and root canal were selected for hematoxylin and eosin (HE) and immunohistochemical staining. Their images were documented by Axio Imager Z1 light microscopy system (Carl Zeiss Co., Ltd., Oberkochen, Germany).

2.7. Enzyme activity staining for ALP and TRACP-5b

Some sections were stained using TRACP-5b/ALP enzyme activity stain kit (FUJIFILM Wako Pure Chemical Corp., Osaka, Japan), which was used to examine the osteoblastic (by ALP) and osteoclastic (by TRACP-5b) cell differentiation and their distribution in the tissue sections, according to the manufacturer's instructions.

2.8. Immunohistochemical staining

The following primary antibodies were used for incubation at 4 °C overnight: mouse monoclonal antibody anti-CD68 antibody (MSB1453, Sigma-Aldrich, St. Louis, USA), dilution 1:50, mouse polyclonal antibody anti- CD163 antibody (MCA342GA, BIORAD, California, USA), dilution 1:50, mouse monoclonal antibody against rat IL-4 (OX81, Santa Cruz Biotechnology, CA, USA), dilution 1:50, mouse monoclonal antibody against rat VEGF (C-1, Santa Cruz Biotechnology, CA, USA), dilution 1:50, and goat polyclonal antibody against rat CD34 (C-18, Santa Cruz Biotechnology, CA, USA), dilution 1:50. The sections were washed with three changes of TBS Tween and incubated with secondary Alexa conjugated anti-IgG antibodies such as Alexa 448 (green) and 647 (NIR) according to the manufacturer's instructions. Fluorescent images were visualized using an Axio Imager Z1 (Carl Zeiss, Oberkochen, Germany), according to the manufacturer's instructions.

2.9. Statistical analyses

Difference in root apex radiolucency volumes among Pg-1w, Pg-2w, and Ctrl specimens were analyzed by Kruskal-Wallis and Mann-Whitney U-tests with Bonferroni correction for alpha ($p \leq 0.016$), using Soft IBM SPSS Statistics 27.

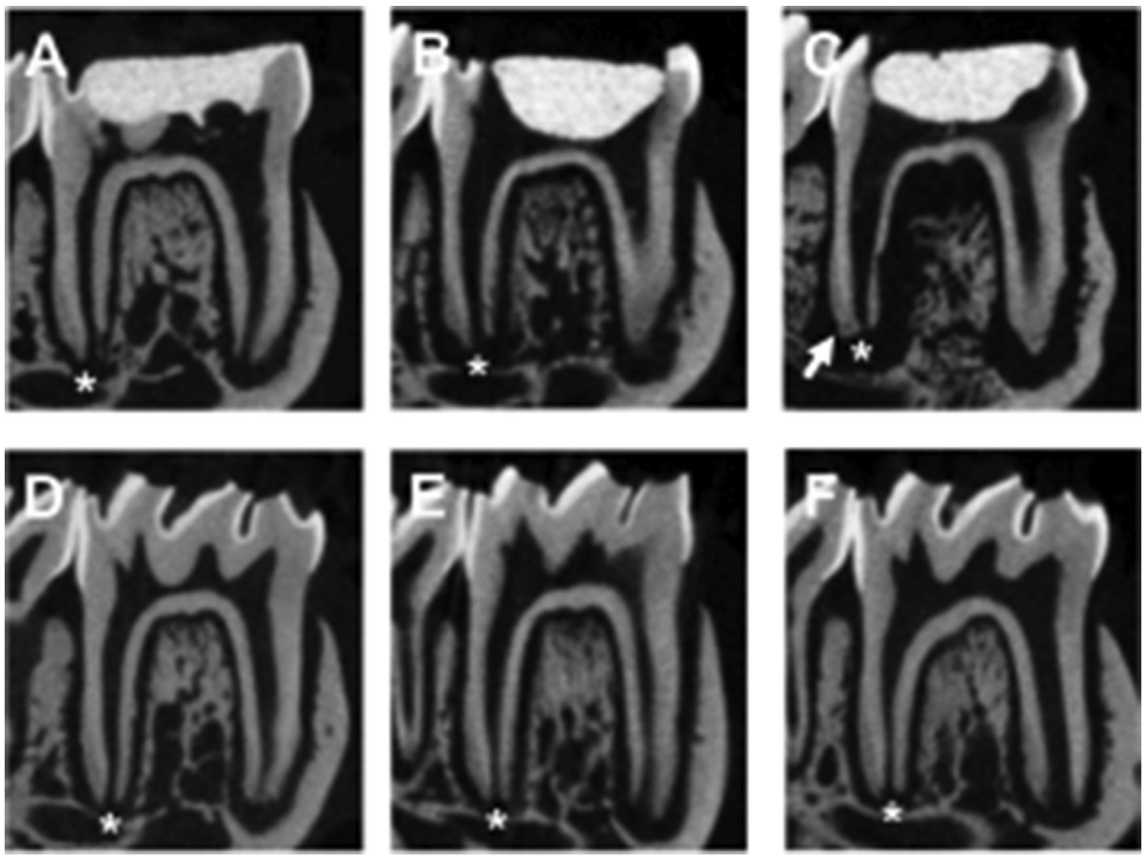

Fig. 2 – Micro CT images of mandibular first molar. Micro CT images revealing mean volumes of distal root apex lesions: A; Ctrl (Vehicle), B; Pg-1w, C; Pg-2w, D; Intact Ctrl, E; Intact Pg-1w (Opposite side of Pg-1w), F; Intact Pg-2w (Opposite side of Pg-2w). Asterisks (*) indicated the root apex of distal root. Arrow indicated cementum hypertrophy. Alveolar bone resorption was more intense and extensive in Pg-1w and Pg-2w than Ctrl.

Please cite this article as: Nakajima C et al., Progress of LPS-induced apical lesion in rat immature mandibular molars, Pediatric Dental Journal, https://doi.org/10.1016/j.pdj.2022.12.001

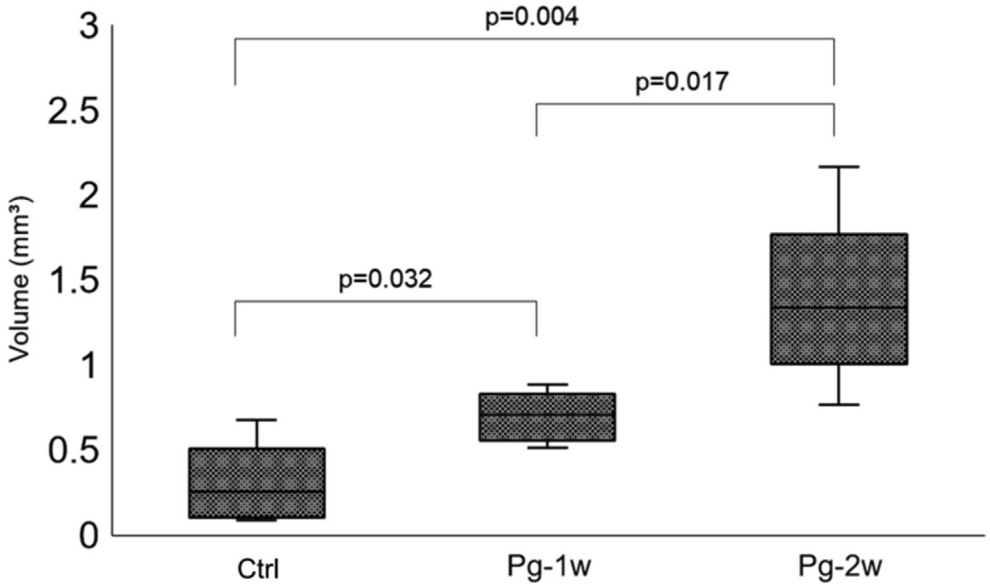

Fig. 3 – Mean volumes of distal root apex foci. Box plot showing comparisons between Ctrl, Pg-1w and Pg-2w volumes. All data are presented as the mean ± SD. Significance probability p-values were corrected by Bonferroni's correction ($p < 0.016$). There was a statistically significant difference between Ctrl and Pg-2w volumes.

3. Results

3.1. *Operating table*

Since the operating table allowed adjustment of the fixation table angle, a good operative field was easily obtained. The rat mouth was kept open, the rubber dam isolation prevented moisture (Fig. 1B), and fixation stabilized the mandible. Operations in mandibular molars were performed with no damage to the oral cavity and the mandible kept stable and secure for 30 min (Fig. 1C). The device allowed fine adjustment of the incisor traction portion and the left and right buccal mucosa traction portions in four directions (Fig. 1D, E). The device facilitated surgery by keeping the mouth open and ensuring a good stable operative field.

3.2. *Three-dimensional measurement of root canal lesion volume*

Fig. 2 shows micro-CT images of mandibular first molars with much larger radiolucent areas of root apex in treated than Ctrl (vehicle control) rats, the latter being almost intact compared with that of no-treatment "Intact" opposite side; distal canal lesion mean volume was 0.67 mm3 in Pg-1w, 1.34 mm3 in Pg-2w, and 0.30 mm3 in Ctrl rats (Fig. 3), with that in Pg-2w being significantly greater than that in Ctrl ($p = 0.004$). Pg-2w showed cementum hypertrophy and transmission images to furcation area. The root was gently enlarged, with no enlargement of the periodontal lumen.

3.3. *Protein array*

The concentrations of the recovered proteins are shown in Table 1. Proteins were recovered in the order of Ctrl-4, Ctrl-3, Pg-2, and Pg-1. Protein recovery patterns differed between Ctrl and Pg groups. Tissue protein analysis of the root apex together with the surrounding alveolar bone resorption area provided protein profiles in this model of apical periodontitis. To assess which proteins were expressed, a root apex map was created with 500 rat protein antibodies. Relative expression levels above 1.85-fold and below 0.87-fold are listed in the order of significance in Table 2. Relevant information of each protein was listed in the last column.

3.4. *Enzyme activity staining for ALP and TRACP-5b*

ALP-positive cells of dark red to purple staining and TRACP-5b-positive cells of pink staining showed distinct distributions (Fig. 4). ALP-positive cells were apparent in alveolar bone sections of Pg-2w and in root apex of Ctrl. Distinct TRACP-5b positive cells were found in the alveolar region of Pg-2w teeth. Ctrl showed higher activity of ALP-positive cells than TRACP-5b-positive cells, and Pg-2w showed ALP-positive cells and TRACP-5b-positive cells at the same site in the alveolar region.

Table 1 – Tissue proteins recovered from the root apex and alveolar bone lesion. More proteins were recovered from the Ctrl groups than the Pg groups. Protein recovery varied from sample to sample.

	amount of protein (μg)			
	Pg-1	Pg-2	CTL-1	CTL-2
First extract	222.48	304.89	453.05	1056.95
Second extract	108.3	326.55	355.87	446.06
Third extract	68.41	83.57	413.47	337.78
Total	399.19	715.01	1222.39	1840.79

Please cite this article as: Nakajima C et al., Progress of LPS-induced apical lesion in rat immature mandibular molars, Pediatric Dental Journal, https://doi.org/10.1016/j.pdj.2022.12.001

Table 2 – Tissue protein analysis of the root apex and alveolar bone lesion. RayBio® label-based antibody array was used to analyze relative expression variations of 500 rat proteins. Some 33 proteins in the Pg-2w samples showed relative expression levels 1.85-fold greater than did vehicle Ctrl samples (A), and some 32 proteins less than 0.87-fold (B). In Table 2A, the darker the red color the higher the expression level, whereas in Table 2B, the same is true for the blue color. URLs for the relevant information was provided in the last column.

		Av	1	2	3	4	DOI
1	pIgR						DOI: 10.1016/j.dci.2021.104072
2	beta 2-M						DOI: 10.1093/biomethods/bpw
3	Smad 3						DOI: 10.1074/jbc.M302566200
4	Annexin A1						DOI: 10.1172/JCI124635.
5	ER alpha						DOI: 10.1002/jbm4.10657
6	FABP5						DOI: 10.1038/s41467-02
7	Cystatin C						DOI: 10.1189/jlb.3A1016-433R
8	Decorin						DOI: 10.1016/j.nbd.2013.12.008
9	NEDD8						DOI: 10.1016/j.bbrc.2013.02.028. Epub 2013 Feb 14.
10	MIP-3 beta						http://www.jimmunol.org/content/161/5/2580
11	TDP-43						DOI: 10.1111/jre.12227. Epub 2014 Sep 9.
12	ILK						DOI: 10.1007/s00018-021-04104-1
13	Galectin-1						DOI:10.1093/glycob/cw1025
14	SOX2						DOI: 10.1515/hsz-2014-0317.
15	FKBP51						DOI: 10.1046/j.0902-4441.2003.00204.x
16	Fgr						DOI: 10.1172/jci.insight.139987.
17	KLKB1						DOI: 10.3389/fphar.2021.71511
18	MKK6						DOI:10.1186/1476-9255-11-14
19	GFRA1						DOI:10.1371/journal.pone.0012
20	ALCAM						DOI: 10.1371/journal.pone.0243272
21	Nestin						DOI: 10.1111/jre.12229. Epub 2014 Sep
22	LPHN3						DOI: 10.3892/etm.2017.5376
23	p27						DOI: 10.1016/j.dnarep.2018.07.008
24	MCAM						DOI: 10.1007/s10585-016-9801-2.
25	Cathepsin L						DOI: 10.1111/iej.13472.
26	IL-4						DOI: 10.1016/j.jprot.2020.104080.
27	IGFBP-5						DOI: 10.1111/dgd.12632
28	CRYAB						DOI: 10.1007/s12192-018-0941-y
29	HSP70						DOI: 10.1016/j.joen.2017.01.030.
30	Calcineurin B						DOI: 10.1016/0092-8674(94)90253-4.
31	HSP27						DOI: 10.1097/00004770-200102000-00007.
32	PON3						DOI: 10.1096/fj.14-260570
33	Cathepsin B						DOI: 10.1111/j.1600-0765.1992.tb02087.x

(A) ≦1.85 1.85<≧2.0 2.0<≧3.41 3.41<

		Av	1	2	3	4	DOI
1	VSIG1						DOI: 10.1002/jso.22150
2	Plexin A4						DOI: 10.1084/jem.20101138
3	TIM-1						DOI: 10.4049/jimmunol.1402632
4	UCH-L1						DOI: 10.7150/thno.39814. eCollection 2020.
5	TNF-R1						DOI: 10.1016/S1043-4666(03)00117-0
6	UNC5H1						DOI: 10.1074/jbc.M300415200
7	TrkC						DOI: 10.1016/j.ydbio.2018.07.022
8	NFATC3						DOI: 10.1016/j.bbrc.2018.03.182. Epub 2018 Apr 10.
9	SIRP alpha						DOI: 10.1053/j.seminoncol.2020.05.009. Epub 2020 May 30.
10	Neuroplastin 65						DOI: 10.3389/fncel.2017.00110
11	SIGNR1						DOI: 10.1093/intimm/dxh264. Epub 2005 May 20.
12	Neurogranin						DOI: 10.1089/neu.2019.6759
13	PTK7						DOI: 10.1038/emboj.2011.236.
14	TGM2						DOI 10.1007/s00726-015-2039-5
15	SOX10						DOI: 10.1111/jre.12229
16	TIE-2						DOI: 10.1016/j.bbrc.2019.01.079
17	SH2B1						DOI: 10.1016/j.bbagen.2014.08.011
18	TRHDE						DOI: 10.1007/s10735-021-09968-y. Epub 2021 Mar 6.
19	Secretagogin						DOI: 10.1073/pnas.1700662114. Epub 2017 Feb 21.
20	Calcineurin A						DOI: 10.1002/jcp.30255. Epub 2021 Jan 3.
21	4-1BB						DOI: 10.3892/etm.2016.3503
22	Ephrin-B2						DOI: 10.1016/j.yexcr.2021.112505
23	Neurofascin						DOI: 10.1016/j.expneurol.2013.05.005. Epub 2013 May 18.
24	p38 gamma						DOI: 10.1083/jcb.200907037
25	SP-D						DOI 10.1007/s00418-009-0609-x
26	Alpha-Synuclein						DOI: 10.1186/s12974-019-1658-2.
27	MAG						DOI: 10.1006/mcne.1997.0633.
28	TWEAK R						DOI: 10.1074/jbc.M302518200
29	TAFA5						DOI: 10.3892/mmr.2019.10724
30	Noggin						DOI: 10.3390/cells9040927.
31	CD47						DOI: 10.1080/2162402X.2017.1391973
32	MIF						DOI: 10.2174/1389557515666150203143317

(B) ≦0.4 0.4<≧0.5 0.5<≧0.87 0.87<

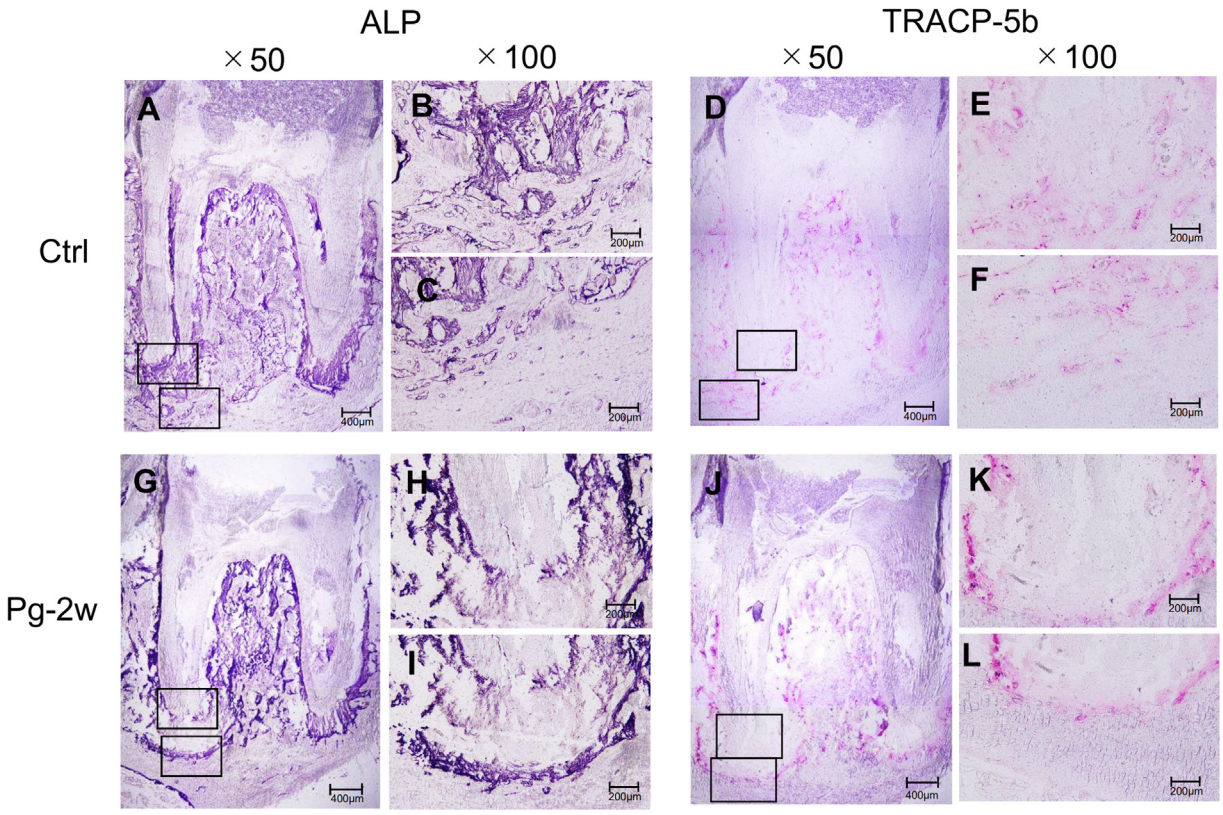

Fig. 4 – Enzyme activity staining for ALP and TRACP-5b after 2-week incubation. Frozen sections of periapical areas were stained for ALP for osteoblastic cells and TRACP-5b enzyme activity for cells of osteoclast lineage. Images indicated ALP-positive Ctrl (x50 (A) and x100 (B) of apical area and x100 of alveolar bone area (C)) and Pg-2w (x50 (G) and x100 (H) of apical area and x100 of alveolar bone area (I)). Similarly, TRACP-5b-positive Ctrl (x50 (D) and x100 (E) of apical area and x100 of alveolar bone area (F)) and Pg-2w (x50 (J) and x100 (K) of apical area and x100 of alveolar bone area (L)). Numbers are original magnifications. Areas in the black box in A, D, G and J were separately enlarged and shown in B, C, E, F, H, J and K at a higher magnification on the right. Black bars indicate 400 μm (A, D, G and J) and 200 μm in all others.

Please cite this article as: Nakajima C et al., Progress of LPS-induced apical lesion in rat immature mandibular molars, Pediatric Dental Journal, https://doi.org/10.1016/j.pdj.2022.12.001

3.5. *Immunohistochemical staining*

CD68 was highly expressed in Pg-1w and subsided by 2 weeks (Pg-2w). CD163, in contrast, was more highly expressed in Pg-2w than Ctrl and Pg-1w (Figs. 5 and 6). IL-4 expression was stronger in Pg-1w than Ctrl, especially in the root apex and alveolar bone resorption areas (Fig. 7). VEGF expression was stronger in Pg-1w than in Ctrl, especially in the root apex and alveolar bone resorption areas (Fig. 8B and F). CD34 expression was weaker in Ctrl than Pg-1w (Fig. 8C and G) and strong expression was observed from week 1–2 in Pg groups (Fig. 8G and K). In the VEGF and CD34 overlay image, Pg-1w showed more greenish than did Ctrl (Fig. 8D and H).

4. Discussion

Root canal treatment of immature permanent teeth in young children, especially of necrotic teeth, is a major challenge with poor prognosis. Although the efficacy of NSAIDS, concentrated growth factors (CGF), and dentin mesenchymal stem cells (DMSC) have been suggested, there has been a lack of major progress in research, mainly due to a lack of appropriate experimental animal models for suitable statistical analysis.

Animal models are indispensable, not only to investigate drugs being developed but to evaluate certain pathogenesis, and interventions prior to clinical trials. To date, dental experiments have often used rat maxillary molars [6–8] rather than mandibles. While few studies have used mandibular teeth, clinical conditions such as central tubercle fracture necessitate the use of mandibular teeth models to reproduce conditions similar to those in human patients. Use of maxillary molars may pose a risk of damage to pericranial tissues in young and small rats. Therefore, we developed an operation table to facilitate treatments in mandibular molars. Using the novel device, we could successfully study LPS-injected mandibular first molar teeth.

Our results revealed M2 macrophage polarization with expression of proteins suggestive of natural immune responses to periapical infection in immature permanent teeth during a 2-week incubation period after manual inoculation of Pg LPS through the pulp towards the apex. Our aim was to elucidate the natural response to periapical infection in immature teeth. We used LPS injection to avoid complications by unknown bacterial infection that cannot be controlled in the exposed pulp model. Compared to the control vehicle injection, LPS-injection induced significantly larger inflammatory lesions around the apex of first molar tooth roots, both distal and mesial, judged from radiolucent areas in micro CT images (only the former was shown in Fig. 3). We found some hints of reactive ossification to inflammation both in cementum and periosteum in Figs. 2 and 4. To analyze lesion

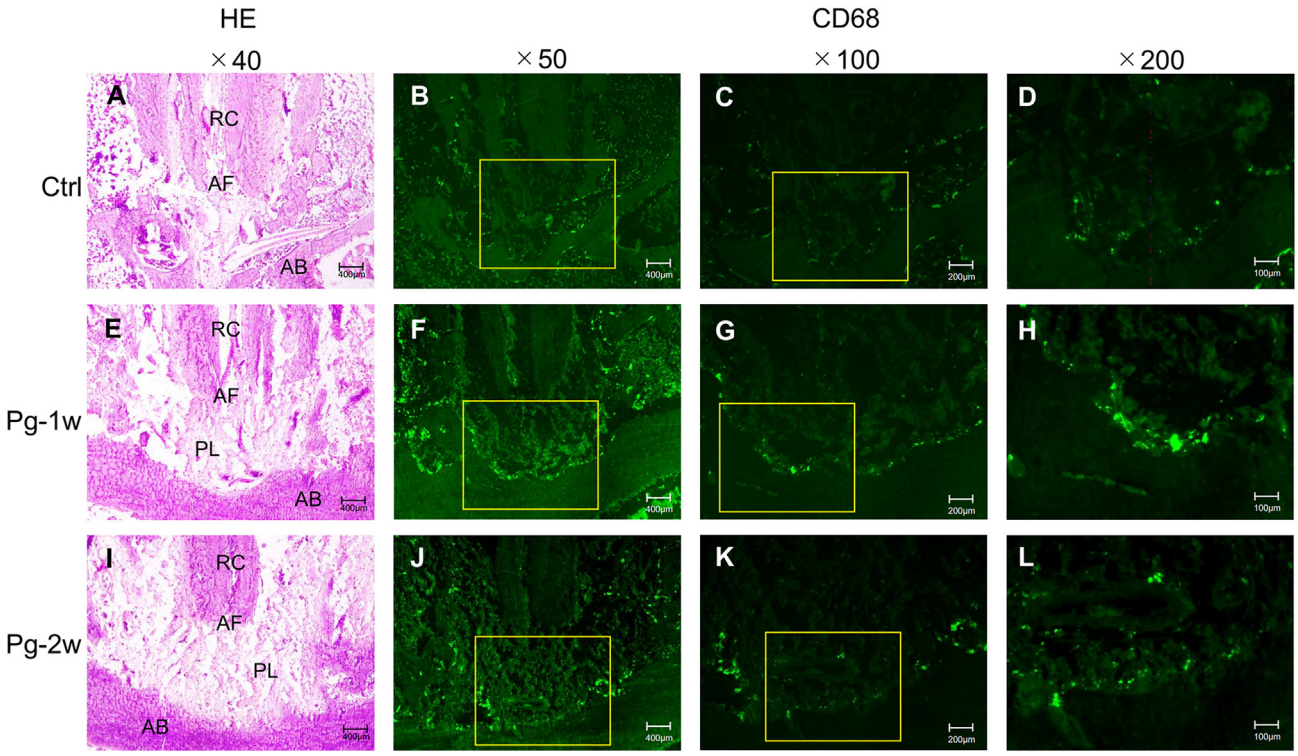

Fig. 5 – Immunofluorescence staining for CD68 and CD163 macrophage cell surface markers of the LPS induced periapical lesions in rats. Serial sections of periapical areas stained with antibodies and hematoxylin and eosin (HE) for Ctrl, Pg-1w and Pg-2w (Figs. 5 and 6). Immunofluorescence staining for CD68 (positive for M1+ and M2± macrophages) (Fig. 5) and CD163 (negative for M1-and positive for M2+ macrophage) (Fig. 6) staining were visualized by secondary Alexa 448 conjugated antibody (green). In Figs. 5 and 6, areas in the yellow boxes were shown separately at a higher magnification. The x100 and x200 images showed the squares inserted in the image magnified at a higher magnification. AF: apical foramen, RC: root canal, PL: periapical lesion, AB: alveolar bone.

Please cite this article as: Nakajima C et al., Progress of LPS-induced apical lesion in rat immature mandibular molars, Pediatric Dental Journal, https://doi.org/10.1016/j.pdj.2022.12.001

tissue protein components, we targeted the lucent area around the distal roots, scraped and recovered the tissue contents with a short bevel (sb) needles, diluted and applied an antibody array of 500 proteins. We used protein-rather than DNA-array because mRNAs do not necessarily represent proteins present in the tissue. In contrast, protein arrays can be directly confirmed by immunohistochemistry for protein localization or by the activity staining. Although the number of available antibodies may be fewer than in DNA arrays, protein array results provide sufficient information to predict a trend. For example, IL4, which induces M2 macrophages, yielded 1.60- to 2.30-fold values and an average of 1.93-fold compared to vehicle controls. The result was in agreement with the immunohistochemical profiles obtained not only with that of IL4 itself but cell surface antibody markers.

Since previous studies showed that systemic responses to osteoclastogenic signaling in mouse apical periodontitis can be seen within 7 and 14 days [13], we examined responses to Pg LPS at 1-week and 2-weeks after inoculation. Induction of resorption was visible by routine X-ray imaging at 1-week (data not shown). Osteogenic as well as osteoclastogenic traits were later confirmed from enzyme activities of ALP and TRACP-5b in frozen sections. Thus, our hypothesis that injecting LPS serves as an apical periodontitis model was confirmed. Although our results are limited by a short 2-week duration, LPS likely induces regeneration of roots even in premature permanent tooth in the presence of M2 macrophages. Previous studies have shown the *in vitro* proliferative effect of 0.1- mg/ml E. Coli LPS via mitogen-activated protein kinase (MAPK) signaling pathways on osteo/odontogenic differentiation of the apical papilla stem cells [14], this LPS-mediated odontogenic differentiation was concentration-dependent and seen neither at 1 μg/ml nor 0.01 μg/ml. A similar concentration-dependent proliferation was reported with TNF-α as well in dental pulp stem cell culture [15] also supporting the self-protective reaction of dental cells. Since odontogenic differentiation of the apical papilla stem cells is prerequisite to root development in immature permanent teeth, it may be assumed that a narrow area of the periapical tissue where LPS was present in a limited range of concentrations provided such an environment for cell proliferation. Our future studies will be extended to the results at longer incubation period with regard to the response we observed at the 14-day.

Throughout life, resident macrophages in most tissues contribute to tissue post-injury responses and immune responses to pathogen assault [16]. Van Furth and Cohn proposed earlier that such resident macrophages develop primarily from circulating, bone marrow-derived blood

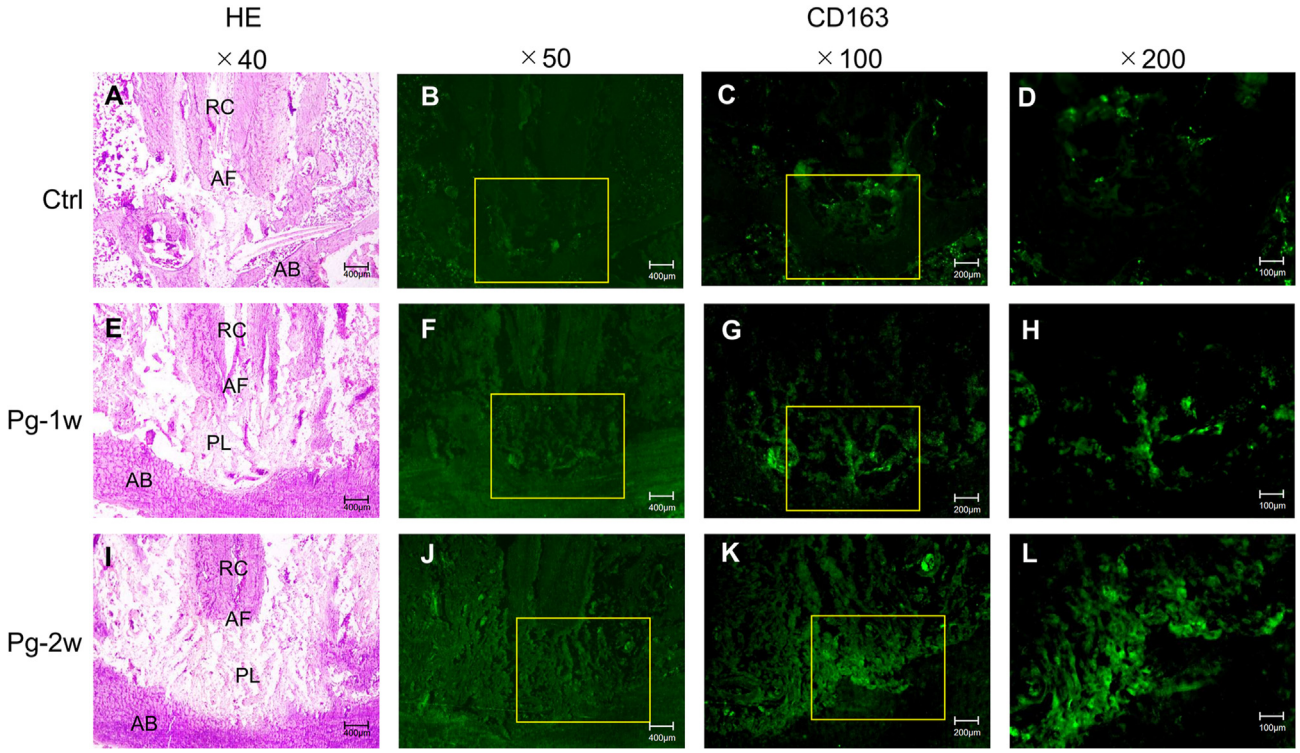

Fig. 6 – Immunofluorescence staining for CD68 and CD163 macrophage cell surface markers of the LPS induced periapicallesions in rats. Serial sections of periapical areas stained with antibodies and hematoxylin and eosin (HE) for Ctrl, Pg-1wand Pg-2w (Figs. 5 and 6). Immunofluorescence staining for CD68 (positive for M1ρ and M2± macrophages) (Fig. 5) andCD163 (negative for M1-and positive for M2ρ macrophage) (Fig. 6) staining were visualized by secondary Alexa 448conjugated antibody (green). In Figs. 5 and 6, areas in the yellow boxes were shown separately at a higher magnification.The x100 and x200 images showed the squares inserted in the image magnified at a higher magnification. AF: apicalforamen, RC: root canal, PL: periapical lesion, AB: alveolar bone.

Please cite this article as: Nakajima C et al., Progress of LPS-induced apical lesion in rat immature mandibular molars, Pediatric Dental Journal, https://doi.org/10.1016/j.pdj.2022.12.001

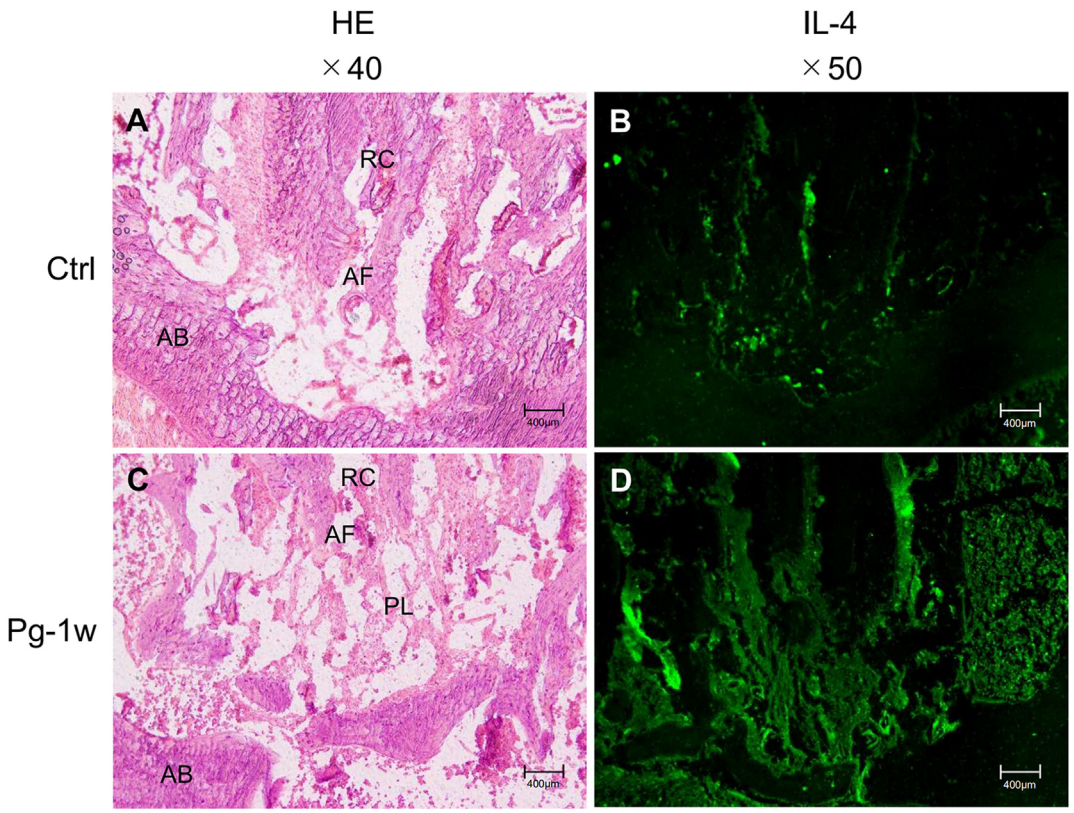

Fig. 7 – Immunofluorescence staining for IL-4 at 1 week. Serial sections of periapical areas were also stained with HE. Immunofluorescence staining for Il-4 was visualized by secondary Alexa 448 conjugated antibody (green). Images indicate cells positive for Il-4 (Ctrl and Pg-1w). AF: apical foramen, RC: root canal, PL: periapical lesion, AB: alveolar bone. (For interpretation of the references to color in this figure legend, the reader is referred to the Web version of this article.)

monocytes [17,18]. This model was widely accepted until recent fate-mapping studies which demonstrated that they arise from other early and late erythro-myeloid progenitors (EMPs) generated in the extra-embryonic yolk sac, for example, during very primitive hematopoiesis [19]. These progenitors can give rise to macrophages without passing through a monocyte stage and are the first to seed the fetal tissues as soon as the blood circulation begins. Except for microglial cells in the brain whose increase was suggested by the protein array experiment, such primitive macrophages in most fetal tissues are subsequently replaced at least partially by fetal liver-derived monocytes. Fetal liver monocytes are generated from EMPs derived from the yolk sac or hemogenic endothelium of maternal origin or from hematopoietic stem cells (HSCs) generated by the embryo. These progenitors are reported to migrate to the fetal liver in waves as EMPs or as immature and mature HSCs giving rise to fetal liver monocytes, which then enter circulation and exodus to differentiate into macrophages in each tissue [20]. Some such macrophages continue self-renewal in each tissue and survive as tissue-resident macrophages. In adulthood they are replaced by bone marrow-derived monocytes generated from hematopoiesis. Resident macrophages are, therefore, a heterogeneous group of cells that support multiple functions. In addition to defense against invading pathogens, they play an essential role in maintaining tissue integrity and homeostasis. For example, 34 osteoclasts are bone-resident macrophages that specialize in bone resorption. Macrophages are able to function depending on their specific locations with unique expression profiles. During regenerative processes such as that in our model, these macrophages encounter diverse stimuli, which change their transcriptional repertoire leading to polarization from M1 to M2 macrophages. M1 macrophage, which is typically induced by LPS or IFN-γ and promotes proinflammatory responses is replaced by M2 macrophage which is induced by IL-4/IL-13, stimulates anti-inflammatory responses [21]. By the protein array assessment, tissue extracts recovered from the areas of periapical lesions at 2 weeks after LPS injection provided us result of doubling IL-4 protein compared to the control extract from the equivalent vehicle-injected area. This result of IL-4, which induces M2 macrophage, suggested the M2 polarization in the lesion at the 2-week-point in our immunohistochemical staining with cell surface marker antibodies of M1 and M2 macrophages, CD68 (M1+, M2±) and CD163 (M1-, M2+) respectively [22].

Although our study could not be extended thus far, different M2 subsets, classified into M2a, M2b, M2c, and M2d, were identified earlier based on the stimuli used for polarization [23]. Even further extended schema of multidimensional macrophages has recently been proposed based on a new extensive gene expression analysis [24]. It is suggested that a spectrum of activation states spanning the M1/M2 types may have occurred in response to LPS we injected and are integrated to determine the overall macrophage response.

Please cite this article as: Nakajima C et al., Progress of LPS-induced apical lesion in rat immature mandibular molars, Pediatric Dental Journal, https://doi.org/10.1016/j.pdj.2022.12.001

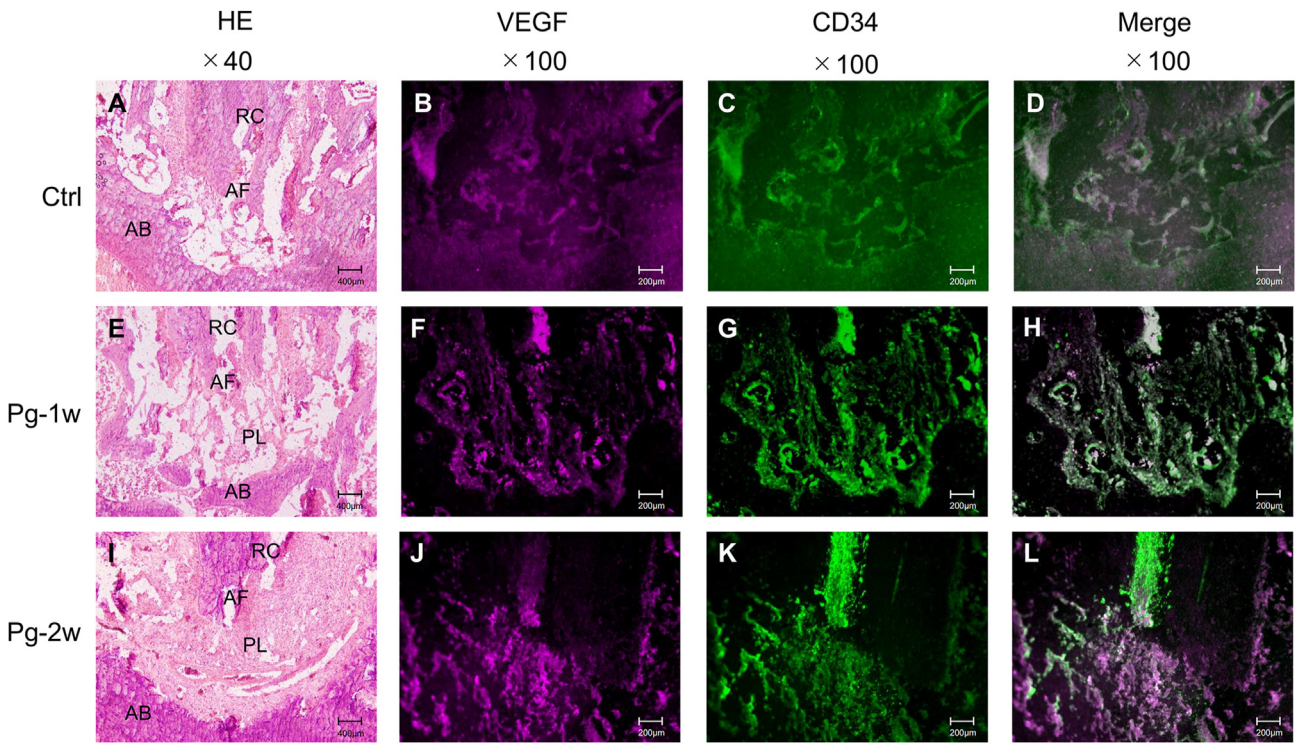

Fig. 8 – Immunofluorescence staining for VEGF and CD34. Serial sections of periapical areas were also stained with HE (x40, A: Ctrl, E: Pg-1w, and I: Pg-2w). Double immunofluorescence staining and overlay of the LPS induced periapical lesions in rats. Immunofluorescence staining for VEGF and CD34 endothelial cell surface marker was conducted around the periapical area, visualized by secondary Alexa conjugated antibodies, Alexa 647 anti-mouse IgG (NIR) and Alexa 448 anti-mouse IgG (green). Images indicate cells positive for VEGF (x100, B: Ctrl, F: Pg-1w, J: Pg-2w), and CD34 (x100, C: Ctrl, G: Pg-1w and K: Pg-2w). The overlay image of Pg-1w suggests VEGF is overwhelming (x100, D: Ctrl, H: Pg-1w and L: Pg-2w). AF: apical foramen, RC: root canal, PL: periapical lesion, AB: alveolar bone. (For interpretation of the references to color in this figure legend, the reader is referred to the Web version of this article.)

We have to admit that this study has certain limitations: it was conducted on rats, which are monophyodont, and not even on canine, which are diphyodont, as in humans. Furthermore, since the findings were obtained in animal experiments, the challenge is to extend to humans. Verification should be conducted at least using animals that are similar to humans. It should be noted that M1 macrophage proteins associated with inflammation, such as IL-6, which are identified in the protein array experiment as increasing x1.5 fold but were reported to have anabolic effects at a later phase, emerged (Data not shown). Since the observation period is limited only up to 2 weeks in this study, individual matrix proteins in the roots, for example, were not identifiable at this point. Also, there are many important proteins not included in the 500 proteins tested.

In clinical practice, it is common to encounter an immature tooth with infected pulp and inflammation that has reached the root of the tooth. Only few studies have been conducted on mineralized tissue induction and root formation at the root apex in immature teeth. By directly applying LPS to the pulp of an immature tooth, we could observe the changes, however. Macrophages that developed over the 2 weeks of treatment have changed in polarity in the transition from inflammation to healing at the protein levels. In the future, we will select those proteins such as Smad3 that increased x3.1 fold, likely involved in mineralized tissue induction and clarify the downstream pathways and proteins involved. Furthermore, we aim to establish drugs and treatment methods to induce root completion by focusing on root apex closure.

5. Conclusion

Our aim was to reveal the elements that promote root completion under conditions in clinically often encountered root-apical periodontitis of immature teeth. In this study, Pg-LPS was injected directly into the apical area of immature teeth, causing apical periodontitis quantitatively. Evaluation of the conditions of the periodontal tissue at the root apex during/after the 2-week procedure provided us useful results showing the process from inflammation to healing. The information provided a clue to root growth and root apical closure of immature teeth, and proved that it was a valuable study that can contribute to the development of new treatment methods.

Declaration of competing interest

The authors declare that they have no conflict of interest.

Please cite this article as: Nakajima C et al., Progress of LPS-induced apical lesion in rat immature mandibular molars, Pediatric Dental Journal, https://doi.org/10.1016/j.pdj.2022.12.001

Acknowledgment

This work was supported by JSPS KAKENHI Grant Number 21K17193 to MFO. We are grateful to Drs. K Muromachi, N Tani-Ishii and N Muto for their valuable suggestions during the course of this study.

REFERENCES

[1] Nagasaka N, Kaihara Y, Okada R, Awane S, Matsushita A, Miura I, et al. A transverse investigation into the immature permanent teeth of Japanese children -degree of eruption, developmental disturbance of tooth structure, and the pattern of occlusion. The Japanese Journal of Pediatric Dentistry 2000;38:1–13.
[2] Ohno K, Nomura T, Sato A, Omori I. Dens Evaginatus in the permanent dentition and the clinical management. The Japanese Journal of Pediatric Dentistry 1996;34:842–8.
[3] Ishidai R, Mishimai K, Adachii C, Miyamoto A, Oshima R, Amari E, et al. Frequency of the developmental disturbances of tooth structure. The Japanese Journal of Pediatric Dentistry 1990;28:466–85.
[4] Otani H, Nonaka K, Matsumoto T, Yanagita K, Sasaki Y, Bae J, et al. Early detection of Dens Evaginatus appearing on the 1st and 2nd premolars and clinical management. The Japanese Journal of Pediatric Dentistry 1993;31:536–41.
[5] Nakagawa Y, Kanamoto Y, Takei T, Inoue Y, Nishihara Y, Ooshima T, et al. Prognosis of Dens Evaginatus in immature permanent teeth. The Japanese Journal of Pediatric Dentistry 1996;34:1036–43.
[6] Sone PP, Kaneko T, Zaw SYM, Sueyama Y, Gu B, Murano H, et al. Neural regeneration/remodeling in engineered coronal pulp tissue in the rat molar. J Endod 2020;46:943–9.
[7] Trongkij P, Sutimuntanakul S, Lapthanasupkul P, Chaimanakarn C, Wong RH, Banomyong D. Pulpal responses after direct pulp capping with two calcium-silicate cements in a rat model. Dent Mater J 2019;38:584–90.
[8] Minic S, Florimond M, Sadoine J, Valot-Salengro A, Chaussain C, Renard E, et al. Evaluation of pulp repair after biodentine(tm) full pulpotomy in a rat molar model of pulpitis. Biomedicines 2021;9.
[9] Wong J, Manoil D, Nasman P, Belibasakis GN, Neelakantan P. Microbiological aspects of root canal infections and disinfection strategies: an update review on the current knowledge and challenges. Front Oral Health 2021;2:672887.
[10] Tamiya Y, Hamba H, Mitomo K, Furusawa M, Muramatsu T. High-cholesterol condition promotes apical periodontitis and bone resorption in rats. The Hard Tissue Biology Network Association 2021;30:199–204.
[11] Stashenko P, Wang C-Y, Tani-Ishii N, Yu SM. Pathogenesis of induced rat periapical lesions. Oral Surgery, Oral Medicine, Oral Pathology and Oral Radiology 1994;78:494–502.
[12] Hidaka K, Miyamoto C, Kawata A, Saita M, Kawamata R, Maehata Y, et al. Effect of low-intensity pulsed ultrasound on remote bone marrow in rats with healing socket. J Orthop Trauma 2016;30(8):S5–6.
[13] Petean IBF, Almeida-Junior LA, Arnez MFM, Queiroz AM, Silva RAB, Silva LAB, et al. Celecoxib treatment dampens LPS-induced periapical bone resorption in a mouse model. Int Endod J 2021;54:1289–99.
[14] Junqing L, Jing D, Xinyu C, Yan L, Zha W, Song M, et al. The effects of mitogen-activated protein kinase signaling pathways on lipopolysaccharide-mediated osteo/odontogenic differentiation of stem cells from the apical papilla. Int Endod J 2019;45:161–7.
[15] He W, Wang Z, Luo, Yu Q, Jiang Y, Zhang Y, et al. LPS promote the odontoblastic differentiation of human dental pulp stem cells via mapk signaling pathway. J Cell Physiol 2014;230:554–61.
[16] Laskin DL, Sunil VR, Gardner CR, Laskin JD. Macrophages and tissue injury: agents of defense or destruction? Annu Rev Pharmacol Toxicol 2011;51:267–88.
[17] Ralph F, Zanvil AC. The origin and kinetics of mononuclear phagocytes. J Exp Med 1968;128:415–35.
[18] Slava E, Kory J, Gwendalyn JR. Origin and functions of tissue macrophages. Immunity 2014;41(1):21–35.
[19] Palis J, Chan RJ, Koniski A, Patel R, Starr M, Yoder MC. Spatial and temporal emergence of high proliferative potential hematopoietic precursors during murine embryogenesis. Proc Natl Acad Sci USA 2001;98:4528–33.
[20] McGrath KE, Frame JM, Fromm GJ, Konisiki AD, Kingsley PD, Little J, et al. A transient definitive erythroid lineage with unique regulation of the beta-globin locus in the mammalian embryo. Blood 2011;117:4600–8.
[21] Holden JA, Attard TJ, Laughton KM, Mansell A, Simpson NMO, Reynolds E, et al. Porphyromonas gingivalis lipopolysaccharide weakly activates M1 and M2 polarized mouse macrophages but induces inflammatory cytokines. Infect Immun 2014;82:4190–203.
[22] Bertasso AS, Léon JE, Silva RAB, Silvia LAB, Queiroz AM, Pucinelli CM, et al. Immunophenotypic quantification of M1 and M2 macrophage polarization in radicular cysts of primary and permanent teeth. Int Endod J 2020;53:627–35.
[23] Zhou X, Zhang J, Li Y, Cui L, Wu K, Luo H. Astaxanthin inhibits microglia M1 activation against inflammatory injury triggered by lipopolysaccharide through down-regulating miR-31-5p. Life Sci 2021;267:118943.
[24] Krautter F, Recio C, Hussain MT, Lezama DR, Maione F, Chimen M. Characterisation of endogenous Galectin-1 and -9 expression in monocyte and macrophage subsets under resting and inflammatory conditions. Biomed Pharmacother 2020 Oct;130:110595.